over the middle- and high-latitude continents over the past decade (Fig. 2) resemble some results obtained by coupled atmosphere-ocean models forced with steadily increasing atmospheric greenhouse gases (*25*), and evidence suggests that the recent warming may be related to increasing tropical ocean temperatures that have led to an enhancement of the tropical hydrologic cycle (*12*, *26*). However, significant decade-long changes in the atmospheric circulation, and in the NAO in particular, have contributed substantially to the regional warming, complicating the interpretation of the climate system response to increased greenhouse gas forcing. Decadal variability in the NAO has become especially pronounced since about 1950 (Fig. 1A), but the causes for such variability in the Atlantic are not clear. The relation of the NAO to greenhouse gas forcing and possible links to coherent variations in tropical Atlantic SSTs (*27*) need to be examined, along with how well climate models simulate the NAO and its recent variations.

REFERENCES AND NOTES

1. G. T. Walker and E. W. Bliss, *Mem. R. Meteorol. Soc.* **44**, 53 (1932); H. van Loon and J. C. Rogers, *Mon. Weather Rev.* **106**, 296 (1978); J. M. Wallace and D. S. Gutzler, *ibid.* **109**, 784 (1981); A. G. Barnston and R. E. Livezey, *ibid.* **115**, 1083 (1987); Y. Kushnir and J. M. Wallace, *J. Atmos. Sci.* **46**, 3122 (1989). An empirical orthogonal function analysis reveals that the NAO is the dominant mode of variability of the surface atmospheric circulation in the Atlantic and accounts for more than 36% of the variance of the mean December to March SLP field over the region from 20°N to 80°N and 90°W to 40°E during 1899 through 1994. Barnston and Livezey show that the oscillation is present throughout the year in monthly mean data but that it is most pronounced during winter.
2. J. C. Rogers, *J. Clim. Appl. Meteorol.* **24**, 1303 (1985).
3. H. H. Lamb and A. I. Johnson, "Secular variations of the atmospheric circulation since 1750," in *Geophys. Mem.* vol. 110 [Her Majesty's Stationery Office (HMSO), London, 1966]; H. H. Lamb, "British Isles weather types and a register of daily sequence of circulation patterns, 1861–1971," in *Geophys. Mem.* vol. 116 (HMSO, London, 1972); T. J. Makrogiannis, A. A. Bloutsos, B. D. Giles, *J. Climatol.* **2**, 159 (1982); D. E. Parker and C. K. Folland, *Meteorol. Mag.* **117**, 201 (1988).
4. H. van Loon and J. Williams, *Mon. Weather Rev.* **104**, 636 (1976).
5. T. Moses *et al.*, *J. Climatol.* **7**, 13 (1987).
6. K. E. Trenberth, in *Earth System Responses to Global Change: Contrasts Between North and South America*, H. A. Mooney, E. R. Fuentes, B. I. Kronberg, Eds. (Academic Press, New York, 1993), pp. 35–59.
7. The data consist of land surface temperature data from the University of East Anglia [P. D. Jones, *J. Clim.* **1**, 654 (1988)] blended with SST data from the United Kingdom Meteorological Office [M. Bottomley, C. K. Folland, J. Hsiung, R. E. Newell, D. E. Parker, "Global ocean surface temperature atlas" (UK Meteorological Office, London, 1990)].
8. T. Nitta and S. Yamada, *J. Meteorol. Soc. Jpn.* **67**, 375 (1989); K. E. Trenberth, *Bull. Am. Meteorol. Soc.* **71**, 988 (1990).
9. K. E. Trenberth and J. W. Hurrell, *Clim. Dynam.* **9**, 303 (1994).
10. D. R. Cayan, *J. Clim.* **5**, 354 (1992).
11. A. Kitoh, *J. Meteorol. Soc. Jpn.* **69**, 271 (1991); T.-C. Chen, H. van Loon, K.-D. Wu, M.-C. Yen, *ibid.* **70**, 1137 (1992); N. E. Graham, *Clim. Dynam.* **9**, 135 (1994); A. J. Miller, D. R. Cayan, T. P. Barnett, N. E. Graham, J. M. Oberhuber, *ibid.*, p. 287.
12. A. Kumar *et al.*, *Science* **266**, 632 (1994).
13. N. E. Graham *et al.*, *J. Clim.* **7**, 1416 (1994); N.-C. Lau and M. J. Nath, *ibid.*, p. 1184.
14. C. S. Bretherton *et al.*, *ibid.* **5**, 541 (1992).
15. K. E. Trenberth and D. A. Paolino, *Mon. Weather Rev.* **108**, 855 (1980).
16. J. C. Rogers, *J. Clim.* **3**, 1364 (1990); J. W. Hurrell, *J. Atmos. Sci.* **52**, 2286 (1995).
17. K. E. Trenberth, *Nat. Ctr. Atmos. Res. Tech. Note NCAR/TN-373+STR* (National Center for Atmospheric Research, Boulder, CO, 1992); ——— and C. J. Guillemot, *J. Clim.*, in press. The ECMWF data were truncated at 21 wave numbers with a spherical harmonic representation and were available at seven vertical levels. The moisture budget was computed with the vertically integrated equation for conservation of water vapor, ignoring the role of liquid water in the atmosphere and the local rate-of-change term
$$\nabla \cdot \frac{1}{g} \int_0^{P_s} q\mathbf{v}dp = E - P$$
where q is the specific humidity, $\mathbf{v}$ is the horizontal vector wind, and p is pressure; s denotes surface pressure, and g represents gravity.
18. D. H. Bromwich, F. M. Robasky, R. A. Keen, J. F. Bolzan, *J. Clim.* **6**, 1253 (1993).
19. World Glacier Monitoring Service (WGMS), Glacier Mass Balance Bulletin no. 3, 1992–1993 (Zurich, 1994).
20. National Oceanic and Atmospheric Administration (NOAA), Climate Assessment: A Decadal Review 1981–1990 (Government Printing Office, Washington, DC, 1991). Seasonal precipitation anomaly distributions are available from NOAA Annual Climate assessments, from Climate System Monitoring (CSM) monthly bulletins produced by the World Climate Programme, and from NOAA monthly climate diagnostics bulletins.
21. C. U. Hammer *et al.*, *Radiocarbon* **28**, 284 (1986); W. Dansgaard *et al.*, *Nature* **339**, 532 (1989); K. C. Taylor *et al.*, *ibid.* **361**, 432 (1993); R. B. Alley *et al.*, *ibid.* **362**, 527 (1993).
22. L. K. Barlow *et al.*, *Geophys. Res. Lett.* **20**, 2901 (1993).
23. J. Bjerknes, *Adv. Geophys.* **10**, 1 (1964); C. Deser and M. L. Blackmon, *J. Clim.* **6**, 1743 (1993); Y. Kushnir, *ibid.* **7**, 141 (1994).
24. S. Levitus *et al.*, *Science* **266**, 96 (1994).
25. Intergovernmental Panel on Climate Change (IPCC), *Climate Change 1992: The Supplementary Report to the IPCC Scientific Assessment*, J. T. Houghton, B. A. Callander, S. K. Varney, Eds. (Cambridge Univ. Press, Cambridge, 1992).
26. N. E. Graham, *Science* **267**, 666 (1995).
27. N.-C. Lau and M. J. Nath, *J. Clim.* **3**, 965 (1990).

28. The ECMWF data were provided by ECMWF. The comments of two anonymous reviewers helped improve the manuscript. Special thanks to K. Trenberth and H. van Loon for their scientific guidance and useful comments and suggestions. The National Center for Atmospheric Research is sponsored by NSF.

20 March 1995; accepted 30 May 1995

Rescue of the *En-1* Mutant Phenotype by Replacement of *En-1* with *En-2*

Mark Hanks,* Wolfgang Wurst,† Lynn Anson-Cartwright, Anna B. Auerbach,‡ Alexandra L. Joyner‡§

The related mouse *Engrailed* genes *En-1* and *En-2* are expressed from the one- and approximately five-somite stages, respectively, in a similar presumptive mid-hindbrain domain. However, mutations in *En-1* and *En-2* produce different phenotypes. *En-1* mutant mice die at birth with a large mid-hindbrain deletion, whereas *En-2* mutants are viable, with cerebellar defects. To determine whether these contrasting phenotypes reflect differences in temporal expression or biochemical activity of the En proteins, *En-1* coding sequences were replaced with *En-2* sequences by gene targeting. This rescued all *En-1* mutant defects, demonstrating that the difference between *En-1* and *En-2* stems from their divergent expression patterns.

The mouse *Engrailed* (*En*) genes *En-1* and *En-2* are the murine members of a large conserved gene family related to the *Drosophila* segmentation gene *engrailed* (*en*). All En genes encode proteins that contain a homeodomain as well as four small, highly conserved regions (*1*). However, outside these regions, En proteins share little identity across the phyla. Overall, En-1 and En-2 proteins share approximately 55% amino acid identity with each other and approximately 35% identity with *Drosophila* En protein.

En-1 expression is first detected during mouse embryogenesis at the one-somite stage, in cells of the anterior neural folds. *En-2* expression, which occurs in a similar region, initiates at the five-somite stage but does not fully overlap with *En-1* until approximately eight somites have formed (*2*). Expression of both genes continues in cells of the ventricular layer of this presumptive mid-hindbrain region. At 9.5 days post coitus (dpc), *En-1* expression

Division of Molecular and Developmental Biology, Samuel Lunenfeld Research Institute, Mt. Sinai Hospital, Toronto M5G 1X5, Canada.

*Present address: Procter and Gamble Pharmaceuticals, Miami Valley Laboratories, Cincinnati, OH 45253–8707, USA.

†Present address: GSF Research Center, Institute for Genetics, Ingolstaedter Landstrasse 1D-85758, Oberschleissheim-Munich, Germany.

‡Present address: Developmental Genetics Program, Skirball Institute of Biomolecular Medicine, New York University Medical Center, 540 First Avenue, New York, NY 10016, USA.

§To whom correspondence should be addressed.

also is detectable in two ventrolateral stripes in the hindbrain and spinal cord, in the dermomyatome, in the ventral ectoderm of the limb buds, and in sclerotomes (3).

En-1 and *En-2* are key regulators of neural development, and *En-1* also plays a crucial role in normal patterning of the limbs and skeleton. *En-2* mutant homozygous mice are viable and fertile but show an embryonic reduction in cerebellar size and postnatal alteration of foliation (4). In contrast, *En-1* mutants ($En\text{-}1^{hd/hd}$; *hd*, homeobox deletion) do not feed and die within 24 hours after birth (5). $En\text{-}1^{hd/hd}$ mutants exhibit a deletion of cells from the presumptive mid-hindbrain region that is obvious by 9.5 dpc, which results in loss of the third and fourth cranial nerves and of most of the colliculi and cerebellum. Skeletal defects of the limbs, 13th rib, and sternum also are apparent.

Two obvious hypotheses could explain the difference between the *En-1* and *En-2* mutant brain phenotypes, given the extensive overlap in protein expression and their high degree of stuctural similarity. First, in spite of their similar structure, these proteins may have acquired novel biochemical functions during evolution and so fulfill different roles within the same cells. Alternatively, the proteins could be biochemically equivalent, but the divergence in the temporal expression pattern between the two genes may have resulted in the expression of a single *En* gene, *En-1*, at the one- to six-somite stage (approximately). Hence, a mutation of *En-2* would be largely compensated for by the presence of *En-1*, but not the converse.

In order to distinquish between these two hypotheses, we used homologous recombination in embryonic stem (ES) cells to functionally replace *En-1* with either *En-2* or with *lacZ* (as a control) by inserting their coding sequences into the *En-1* locus (6). The targeting event brought the integrated sequences under the control of the *En-1* promoter and endogenous regulatory elements and at the same time introduced a null mutation in *En-1* [the knock-in (KI) approach; Fig 1]. We designate these new *En-1* alleles $En\text{-}1^{2ki}$ (*2ki*, *En-2* knock-in) and $En\text{-}1^{Lki}$ (*Lki*, *lacZ* knock-in), respectively. Three ES cell clones targeted with *En-2* and 14 clones targeted with *lacZ* were identified by Southern (DNA) blot analysis (Fig. 1).

Chimeric embryos derived from two *lacZ* targeted ES cell lines were stained directly with X-Gal (7) at 8.0, 9.0, and 11.5 dpc. *lacZ* expression was observed in the anterior neural folds of 8.0-dpc chimeras (8) and in

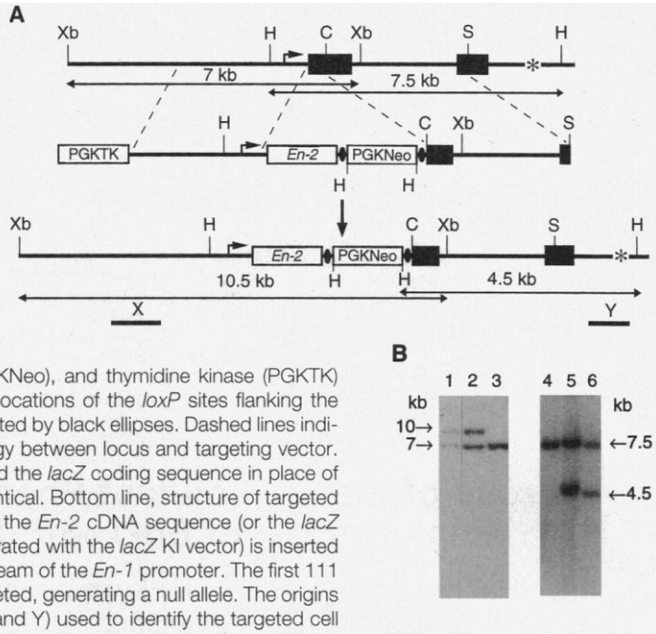

Fig. 1. KI targeting strategy. (**A**) Top line, schematic of the *En-1* genomic locus. The *En-1* promoter is indicated by the horizontal arrow, and the coding sequence flanking the single intron is shown by the black boxes. The asterisk represents the *En-1* polyadenylation signal. Middle line, linearized *En-2* KI vector. The *En-2* coding sequence, selectable neo- mycin resistance (PGKNeo), and thymidine kinase (PGKTK) cassettes are shown. The locations of the *loxP* sites flanking the PGKNeo cassette are depicted by black ellipses. Dashed lines indicate the regions of homology between locus and targeting vector. The *lacZ* KI vector contained the *lacZ* coding sequence in place of *En-2* but was otherwise identical. Bottom line, structure of targeted locus. After gene targeting, the *En-2* cDNA sequence (or the *lacZ* sequence in lines electroporated with the *lacZ* KI vector) is inserted into the *En-1* locus downstream of the *En-1* promoter. The first 111 amino acids of *En-1* are deleted, generating a null allele. The origins of the 5′ and 3′ probes (X and Y) used to identify the targeted cell lines are shown. C, Cla I; H, Hind III; S, Sac I; and Xb, Xba I. (**B**) Southern blots of genomic DNA isolated from targeted ES cell lines. In lanes 1 to 3, DNA was digested with cell Xba I and probed with X (1.2-kb Xho I fragment; internal probe), giving an endogenous 7-kb fragment and targeted 12.2-kb fragment for *lacZ*-targeted cell lines and a 10.5-kb fragment for *En-2*–targeted cell lines (the 12.2- and 10.5-kb mutant bands appear to co-migrate because they were derived from different gels; the 10-kb marker refers to lanes 2 and 3). Lane 1, *lacZ*-targeted line; lane 2, *En-2*–targeted line; lane 3, wild-type ES cells. In lanes 4 to 6, DNA was digested with Hind III and probed with Y (700-bp Eco RI–Hind III fragment; external probe), giving a wild-type 7.5-kb fragment and targeted 4.5-kb fragments for both targeted cell lines. Lane 4, wild-type R1 ES cells; lane 5, *En-2*-targeted line; lane 6, *lacZ*-targeted line.

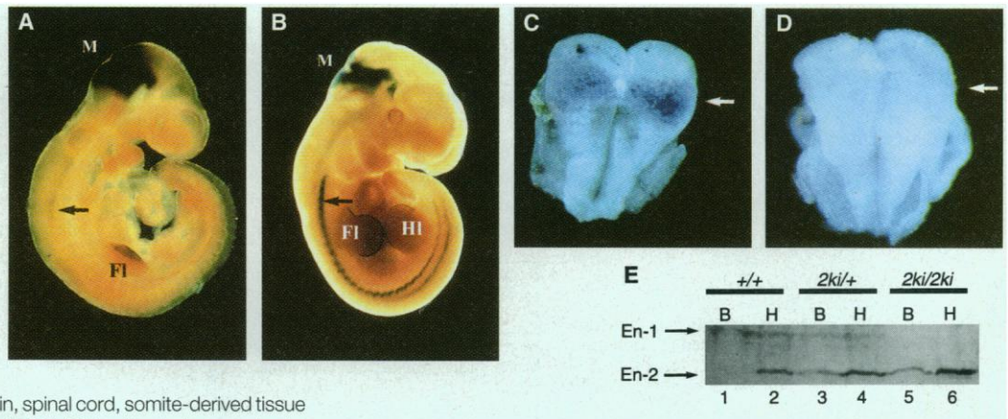

Fig. 2. Expression of integrated *lacZ* and *En-2* sequences in embryos derived from *lacZ*-targeted and *En-2*–targeted ES cell lines, respectively. (A) and (B) show expression of *lacZ* in chimeric embryos derived from aggregation of a *lacZ*-targeted ES cell line with a wild-type morula. (**A**) A 9.0-dpc chimeric embryo stained with X-Gal. Strong expression is seen in the mid-hindbrain region (M) and ventral ectoderm of the forelimb bud (Fl). The few somitic cells staining at this point are indicated by an arrow. (**B**) An 11.5-dpc chimeric embryo stained with X-Gal. *lacZ* expression is seen in the mid-hindbrain region, posterior hindbrain, spinal cord, somite-derived tissue (arrow), forelimb buds (Fl), and hindlimb buds (Hl). (**C**) In situ whole mounts of a one- to two-somite $En\text{-}1^{2ki/+}$ embryo and (**D**) a wild-type embryo probed with an *En-2*–specific antisense sequence. *En-2* expression is seen in the anterior neural folds of the $En\text{-}1^{2ki/+}$ embryo but not the wild-type stage-matched control. A portion of the extra embryonic membranes remaining after dissection was removed from the image with Adobe Photoshop. (**E**) Protein immunoblot of protein extracts prepared from 9.5-dpc embryonic heads (H) and bodies (B), probed with *Enhb-1* antiserum. Lanes 1 and 2, wild-type; lanes 3 and 4, $En\text{-}1^{2ki/+}$; lanes 5 and 6, $En\text{-}1^{2ki/+2ki}$ embryos. En-2 protein is detected in both heads and bodies of $En\text{-}1^{2ki/+}$ and $En\text{-}1^{2ki/+2ki}$ embryos, but only in the head of the wild-type embryos, and no En-1 protein is detected in $En\text{-}1^{2ki/+2ki}$ embryos.

the mid-hindbrain, spinal cord, somites, and limbs of 9.0-dpc and 11.5-dpc chimeras (Fig. 2, A and B). Thus, the integrated *lacZ* sequence was accurately regulated in an *En-1*–specific fashion, a result that was not obtained with a conventional transgenic approach using *En-1* promoter fragments to drive transgenes (*8*).

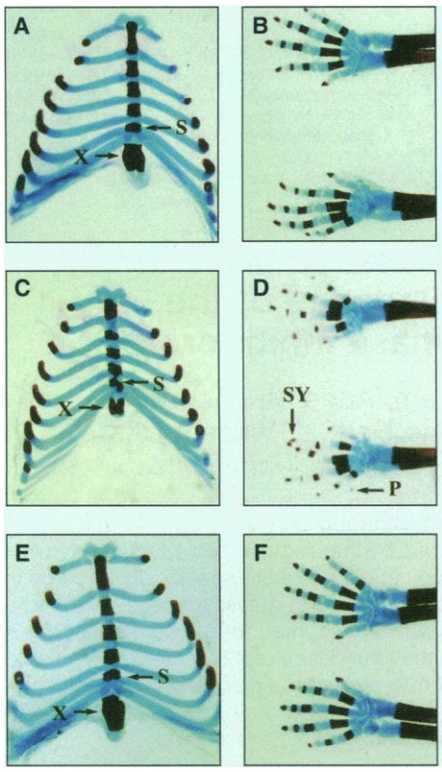

Fig. 3. Alcian blue– (cartilage) and alizarin red– (bone) stained sternums and limbs prepared from (**A** and **B**) wild-type, (**C** and **D**) *En-1*$^{hd/hd}$, and (**E** and **F**) *En-1*$^{2ki/+2ki}$ newborn mice. In (C) and (D), the classic sternum disorganization (S), truncated xiphoid process (X), syndactyly (SY), and postaxial polydactyly (P) present in the *En-1*$^{hd/hd}$ newborn skeleton are indicated with arrows. In (E) and (F), the limbs and sternum of an *En-1*$^{2ki/+2ki}$ pup are indistinguishable from those of the wild-type pup.

Aggregation chimeras giving germline transmission were obtained from one *En-1*^{2ki}–targeted ES cell line. These were bred with *En-1*$^{hd/+}$ heterozygous females to generate *En-1*$^{2ki/hd}$ compound heterozygotes, and F_1 animals interbred to produce *En-1*$^{2ki/2ki}$ homozygous progeny. Mice with either genotype were viable and appeared normal.

To demonstrate that the recombination event had generated an *En-1* null allele, 9.5-dpc embryos were collected from *En-1*$^{2ki/+}$ intercrosses and genotyped. Protein extracts were prepared from individual embryo heads and bodies and analyzed by protein immunoblot with the *Enhb-1* antiserum, which recognizes proteins encoded by both *En-1* and *En-2* (*9*). In wild-type embryos, En-1 (55 kD) and En-2 (41 kD) proteins were detected, as expected, in the head, and En-1 alone was detected in the body (Fig. 2E). *En-1*$^{2ki/+}$ heterozygotes showed En-1 and En-2 protein in both head and body, and *En-1*$^{2ki/2ki}$ homozygous embryos expressed En-2 protein, but not En-1 protein, in the head and body. Thus, the targeting event generated a null allele for *En-1*, and En-2 protein was also present in the body, as expected if expression was controlled by the *En-1* locus.

We confirmed that the pattern of *En-2* expression from the *En-1*^{2ki} allele was like that of *En-1* using whole-mount RNA in situ hybridization (*10*). *En-2* RNA was detected in the anterior neural folds of two-somite-stage *En-1*$^{2ki/+}$ heterozygote embryos (Fig. 2C) but not in two-somite wild-type control embryos (Fig. 2D), although strong expression was detected in the anterior neural folds of six- to seven-somite wild-type embryos (*8*). In 9.5-dpc *En-1*$^{2ki/2ki}$ embryos, En-2 protein was detected with the *Enhb-1* antiserum in the limbs, somites, and spinal cord, as well as in the brain (*8*).

To determine whether expression of En-2 fully rescued the brain and skeletal defects in animals lacking *En-1*, we examined skeletons and brains from newborn *En-1*$^{2ki/+}$ heterozygotes (n = 2), *En-1*$^{2ki/hd}$ compound heterozygotes (n = 4), *En-1*$^{2ki/2ki}$ homozygotes (n = 4), wild-type mice (n = 3), and *En-1*$^{hd/hd}$ (n = 3) mice. In contrast to the disorganized sternums and limbs of *En-1*$^{hd/hd}$ homozygotes (Fig. 3, C and D), the limbs and sternums of *En-1*$^{2ki/hd}$ (*8*) and *En-1*$^{2ki/2ki}$ pups appeared normal (Fig. 3, E and F). Furthermore, *En-1*$^{2ki/2ki}$ homozygous newborn and adult brains appeared identical to those of wild-type littermates in whole-mount preparations and serial sagittal sections (Fig. 4). In summary, the *En-2* and *lacZ* sequences targeted to the *En-1* locus are expressed in *En-1*–specific tissues, and *En-1*$^{2ki/2ki}$ newborn and adult mice that express *En-2* in place of *En-1* appear phenotypically normal.

We have used a KI approach to demonstrate that the two En proteins in the mouse have retained common biochemical functions throughout evolution, by showing that mouse En-2 can substitute for En-1, both in the neural tube in which it is normally expressed as well as in regions, such as the limbs, that normally express only En-1. This is a direct demonstration in mammals of proteins that have acquired novel functions through divergence of gene expression rather than through divergence in biochemical function; a similar demonstration has been reported for *Drosophila* (*11*).

Taken together with the En-1 and En-2 expression data and mutant analysis, the results of our studies allow us to conclude that the deletion of mid-hindbrain struc-

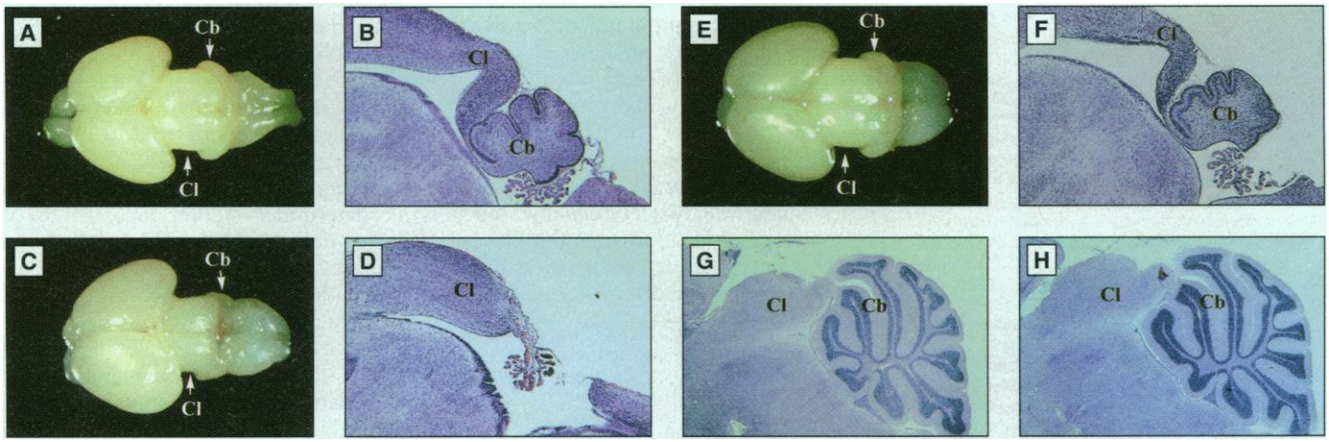

Fig. 4. Analysis of brains from *En-1*$^{2ki/+2ki}$ mice. Intact brains and matched parasagittal sections through brains dissected from wild-type (**A** and **B**), *En-1*$^{hd/hd}$ (**C** and **D**), and *En-1*$^{2ki/+2ki}$ (**E** and **F**) newborn mice are shown. Also shown are matched sagittal sections through cerebellums of 6-week-old *En-1*$^{2ki/2ki}$ (**G**) and wild-type (**H**) mice. Sections were stained with hemotoxylin and eosin. The deletion of colliculi (Cl) and the cerebellum (Cb) are indicated.

tures in *En-1* homozygous mutants is a consequence of a lack of *En* gene function in the anterior neural folds between the one- and eight-somite stages. These results emphasize that early restricted gene expression reflects crucial genetic events that control regional brain development.

The KI approach has broad biological applications. With the appropriate choice of target locus, ectopic expression or gene transplant experiments can be carried out with a degree of control not afforded by the conventional transgenic approach. Such experiments are a necessary complement to elimination of gene function by mutagenesis, because loss of function may serve only to demonstrate that a developmental gene plays a role in the tissue in which it is expressed. Accurately regulated ectopic gene expression in vivo can generate viable mice exhibiting a gain-of-function phenotype (*12*). This can aid in determining the role of the gene in its normal environment or, as in these studies, can clarify the unique and overlapping functions of members of gene families. Because overlapping gene function is likely to be prevalent in mammals, such approaches are critical for determining the complete repertoire of functions of individual genes.

REFERENCES AND NOTES

1. C. Logan *et al.*, *Dev. Genet.* **13**, 345 (1992); A. L. Joyner and M. Hanks, *Semin. Dev. Biol.* **2**, 435 (1991).
2. A. P. McMahon, A. L. Joyner, A. Bradley, J. A. McMahon, *Cell* **69**, 581 (1992).
3. C. A. Davis, S. E. Noble-Topham, J. Rossant, A. L. Joyner, *Genes Dev.* **2**, 361 (1988); C. A. Davis and A. L. Joyner, *ibid.*, p. 1736; D. Davidson, E. Graham, C. Sime, R. Hill, *Development* **104**, 305 (1988).
4. A. L. Joyner, K. Herrup, B. A. Auerbach, C. A. Davis, J. Rossant, *Science* **251**, 1239 (1991); K. J. Millen, W. Wurst, K. Herrup, A. L. Joyner, *Development* **120**, 695 (1994).
5. W. Wurst, A. B. Auerbach, A. L. Joyner, *Development* **120**, 2065 (1994).
6. The *En-1* homologous sequences present in the KI targeting vectors (Fig. 1) were provided by a 4.2-kb Xba I–Apa I 5′ arm containing the *En-1* promoter, together with a 4.0-kb Cla I–Sac I 3′ arm (*5*), flanking either the coding sequence for *En-2* [1.2-kb Eco RI–Bg III fragment (*10*)] or *lacZ* [3.0-kb Eco RI fragment, containing a consensus eukaryotic ATG (S. Darling, unpublished data)] together with the PGK-Neo cassette (*5*). The vectors also carried the herpes simplex virus *TK* gene driven by the PGK promoter (*5*). *loxP* sites were inserted to flank the PGK-Neo cassette to allow CRE-mediated excision of this selectable marker in the event that expression of the targeted *En-1* locus was altered by its presence [R. Hoess, M. Zaise, N. Sternberg, *Proc. Natl. Acad. Sci. U.S.A.* **79**, 3398 (1982); P. C. Orban, D. Chui, J. Marth, *ibid.* **89**, 6861 (1992)]. R1 ES cells (2.5×10^7) [A. Nagy, J. Rossant, R. Nagy, N. W. Abromow, J. C. Roder, *ibid.* **90**, 8424 (1993)] were electroporated with 300 μg of linearized *En-2* or *lacZ* KI vector. After 8 to 9 days of selection in G418 and gancyclovir, approximately 200 double-resistant clones were picked from each experiment, amplified, and screened for the correct targeting event by Southern blot analysis (Fig. 1) [W. Wurst and A. L. Joyner, in *Gene Targeting, A Practical Approach*, A. L Joyner, Ed. (Oxford Univ. Press, Oxford, 1993), pp. 33–61]. Chimeric embryos from *lacZ*-targeted lines were generated by aggregation with diploid or tetraploid morulas, and mouse lines giving germline transmission of the *En-1*^{2ki} allele were established by diploid aggregation [A. Nagy and J. Rossant, *ibid.*, pp. 147–180).
7. C. Logan, W. K. Khoo, D. Cado, A. L. Joyner, *Development* **117**, 905 (1993).
8. M. Hanks and A. L. Joyner, unpublished observations.
9. C. A. Davis, D. P. Holmyard, K. J. Millen, A. L. Joyner, *Development* **111**, 287 (1991).
10. R. A. Conlon and J. Rossant, *ibid.* **116**, 357 (1992). The *En-2*–specific antisense probe was a 1.0-kb Cla I–Bg III fragment derived from the *En-2* complementary DNA (cDNA) [A. L. Joyner and G. R. Martin, *Genes Dev.* **1**, 29 (1987)].
11. X. Li and M. Noll, *Nature* **367**, 83 (1994).
12. M. Kessel, R. Balling, P. Gruss, *Cell* **61**, 301 (1990); M. H. Sham *et al.*, *ibid.* **72**, 183 (1993); M. Zhang *et al.*, *Development* **120**, 2431 (1994); J.Charité, W. De Graf, S. Shen, J. Deshchamps, *Cell* **78**, 589 (1994).

13. We dedicate this work to the memory of M. Breitman, for his enthusiasm, insight, and support. We also thank M. Kownacka and H. Park for technical assistance, S. Chu and K. Harpal for histology, and D. Fawcett and G. Fishell for critical comments on the manuscript. Funded by grants from the Medical Research Council (MRC) of Canada and Bristol-Myers Squibb. A.L.J. was a MRC Scientist and Howard Hughes International Scholar.

12 April 1995; accepted 15 June 1995

Role of the Ubiquitin-Proteasome Pathway in Regulating Abundance of the Cyclin-Dependent Kinase Inhibitor p27

Michele Pagano,* Sun W. Tam, Anne M. Theodoras, Peggy Beer-Romero, Giannino Del Sal, Vincent Chau, P. Renée Yew, Giulio F. Draetta, Mark Rolfe

The p27 mammalian cell cycle protein is an inhibitor of cyclin-dependent kinases. Both in vivo and in vitro, p27 was found to be degraded by the ubiquitin-proteasome pathway. The human ubiquitin-conjugating enzymes Ubc2 and Ubc3 were specifically involved in the ubiquitination of p27. Compared with proliferating cells, quiescent cells exhibited a smaller amount of p27 ubiquitinating activity, which accounted for the marked increase of p27 half-life measured in these cells. Thus, the abundance of p27 in cells is regulated by degradation. The specific proteolysis of p27 may represent a mechanism for regulating the activity of cyclin-dependent kinases.

The cyclin-dependent kinase inhibitor p27 (*1*) is present in maximal amounts during the quiescent (G_0) and prereplicative (G_1) phases of the mammalian cell cycle. The amount of p27 decreases as cells are induced to enter the cell cycle (*2–4*). Unlike all other mammalian cell cycle proteins studied so far, for which correlations have been found between the abundance of these proteins and changes in the amount of mRNA present (*5*), the decline in the amount of p27 occurs in the presence of constant amounts of mRNA and a constant rate of protein synthesis (*3, 4*). Thus, we investigated whether the intracellular regulation of p27 abundance involved the ubiquitin-proteasome pathway (*6*). We examined the effect of the peptide-aldehyde *N*-acetyl-leucinyl-leucinyl-norleucinal-*H* (LLnL), an inhibitor of the chymotryptic site on the proteasome (*7*), on the amount of cellular p27. As a control, we used the cysteine protease inhibitor L-*trans*-epoxysuccinic acid (E64).

Addition of LLnL, but not of E64 or a dimethyl sulfoxide (DMSO) vehicle, induced an accumulation of p27 protein after 60 min of treatment (Fig. 1A). In contrast, p21, another inhibitor of cyclin-dependent kinases, was not found to accumulate appreciably in LLnL-treated MG-63 cells, which lack the gene for the tumor suppressor p53. At later time points, we noticed that two antibodies to p27 that do not recognize the same epitope (*8*) both recognized a doublet with a relative molecular mass (M_r) of ~70,000. The p27 monoclonal antibody (mAb) also recognized a band of M_r ~100,000 in the extract from the 22-hour LLnL time point. To determine whether these bands contained ubiquitinated p27, we immunoprecipitated lysates from LLnL-treated cells with either anti-p27 or control antiserum and then immunoblotted them with a ubiquitin mAb. The M_r 70,000 doublet and a group of slower migrating bands were detected by the ubiquitin mAb exclusively in the anti-p27 immunoprecipitates (Fig. 1A). Immunoblotting with a control antibody of similar immunoprecipitates did not visualize any band (*8*).

M. Pagano, S. W. Tam, A. M. Theodoras, P. Beer-Romero, G. Del Sal, G. F. Draetta, M. Rolfe, Mitotix Inc., 1 Kendall Square, Building 600, Cambridge, MA 02139, USA.
V. Chau, Department of Pharmacology, Wayne State University, Detroit, MI 48201, USA.
P. R. Yew, Department of Cell Biology, Harvard Medical School, Boston, MA 02115, USA.

*To whom correspondence should be addressed.